EXPANSION OF TIME HISTORY RESPONSE MEASUREMENTS FOR VISUALIZATION

Christopher V. White[1], M. B. Levine[1] and M. Ingham[2]

[1] Jet Propulsion Laboratory
4800 Oak Grove Drive, M.S. 157-316
Pasadena, CA 91109, USA

[2] MIT Space Systems Laboratory
77 Massachusetts Avenue, Rm. 37-356
Cambridge, MA 02139, USA

ABSTRACT

To date many methods have been developed to expand measured mode shapes from a limited number of sensors up to the full set of degrees of freedom (DOFs) of an analytical FEM model. Previous papers have evaluated the accuracy of these techniques on actual experimental data [1]. However, many of these methods are limited to the expansion of mode shapes, and often require a priori knowledge of the measured and analytical modal frequencies, as well as pairings between the experimental and analytical modes. These methods cannot be applied to the general case of a measured time history with multi-mode, transient or steady-state response information.

A class of methods for estimating the full state vector from a limited set of measurements, typically used in conjunction with a full-state feedback controller, is an attractive approach for expanding measured time histories. One such method, known as the Kalman filter [2], is a recursive linear state estimator based on least-squares minimization, and can be applied even when measured time histories are noisy or the system dynamics are not known precisely. This paper will explore the methodology of the Kalman filter, and the deterministic counterpart, the Luenberger observer, and evaluate their accuracy on an analytical simulation.

NOMENCLATURE

$\mathbf{x}$ state vector

$\mathbf{y}$ measurement vector

$\mathbf{v}$ noise vector

$\mathbf{A_d}, \mathbf{C_d}$ discrete time system matrices

$\mathbf{R} = E(\mathbf{v}^T\mathbf{v})$ noise covariance matrix

$\hat{\mathbf{x}}$ estimated state vector

$\hat{\mathbf{y}}$ estimated measurement vector

$\mathbf{K}$ feedback gain matrix

$\mathbf{P} = E((\mathbf{x} - \hat{\mathbf{x}})^T(\mathbf{x} - \hat{\mathbf{x}}))$ state error covariance matrix

1. INTRODUCTION

Although static analyses typically use detailed and high-resolution finite element models, reduced-order models (ROM) are popular for dynamic analyses. This is primarily due to the engineering and computational costs of working with models having hundreds, to hundreds of thousands of DOF. Reduced order models are justifiable in many cases because 1) high frequency modes are usually inaccurate in full size models, 2) essential dynamic responses can often be captured using a small number of normal modes. Furthermore, active control design algorithms may not be robust enough to handle large size models, and hence require the use of ROMs, with the understanding that closed-loop performance may need to be checked using the full order model.

Model reduction techniques for structural dynamics can be assigned to one of two groups according to whether truncation takes place in the physical coordinate space (DOFs or nodal points eliminated) or in a generalized coordinate space. Guyan/Irons reduction[4,5], IRS reduction [6], as well as using FE models with lower spatial detail are examples of the first, while normal-mode modal truncation, Krylov or Ritz-vector [7] based models, or balanced gain reduction [8] are examples of the latter.

The inverse procedure is the expansion of the reduced model results up to the full-size model. This is a familiar step in modal analysis where the solution in generalized coordinates is projected to physical coordinates by premultiplication by the mode shape matrix. Likewise, experimentally measured mode shapes can be expanded by various techniques from the measured a-set DOF to the unmeasured o-set DOFs. This is a necessary step for spatially complete mode shape animation or orthogonality and cross-orthogonality checks using the FE model mass and stiffness matrices. Previous studies have shown how to cast these mode shape expansion methods into the framework of minimum-norm operations and assessed their accuracy on experimental data [1]. These methods operate solely on a mode-by-mode basis, i.e., the objective is to expand eigenvectors, not to expand a whole time

history containing responses in various modes. For the Guyan, IRS, and Ritz model reduction methods, the reduction transformation matrix can be used to project time histories at the reduced DOFs onto the omitted DOFs, but this approach can be inaccurate. Problems will arise in projecting measured acceleration time histories to unmeasured nodes and then visualizing structural motions as accelerations, as the high-frequency acceleration components will distort the deflected shapes, unless the time histories contain only a single frequency. On the other hand, if noisy acceleration measurements are double-integrated to displacements, there is a possibility that low-frequency noise will be the largest magnitude in the integrated signal, making the projections meaningless. This is especially relevant when the measured motions of interest are just above the background noise of the instrumentation.

This paper investigates a type of expansion process that potentially has a more general application to transient responses. The animation of the complete structural motion during transient responses can give insight into the structure's behavior during normal service conditions (operational deflected shapes for example), wave propagation events, or dynamic 'snap' events that result from sudden changes in configuration. Especially attractive would be the visualization of the shape just after a snap event has taken place, in order to determine the source location. This is one aspect of current interest in the analysis of the IPEX experimental data [3]. Additional benefits of these techniques include generating smooth estimates of structural motions from noisy measurements, and estimating the motions of unmeasured DOFs for nonlinear structures.

The class of expansion techniques studied here are known as state estimators. The first method considered is the deterministic Luenberger full-state observer, and the second is the Kalman filter. These ideas have been in use for estimating the state vector of dynamical systems in active control since the early 1960's, when published by Luenberger and Kalman [9],[2]. Their implementation has not been wide in the structural dynamics community as of yet. These techniques are investigated to see how successful they might be for estimating the complete displacement vector of a realistic space structure when only a small number of acceleration measurements are made, when the motions are in the μm range, and the responses are of a transient nature.

2. STATE ESTIMATION TECHNIQUES

The state estimation problem consists of constructing an estimate of the time behavior of a dynamical system from potentially noisy measurements of some of the states or possibly independent linear combinations of the states. We consider the discrete-time difference equations of the system and its discrete-time measurement equation:

$$\mathbf{x}(i + 1) = \mathbf{A}_d\mathbf{x}(i) \qquad (1)$$

$$\mathbf{y}(i) = \mathbf{C}_d\mathbf{x}(i) + \mathbf{v}(i) \qquad (2)$$

in which the *2n-dimensional* state vector is $\mathbf{x}$, the *m-dimensional* measurement vector is $\mathbf{y}$, and $\mathbf{v}$ is the measurement noise vector with covariance matrix $\mathbf{R}$. In practical applications, the measurements consist of accelerations, which are state derivatives, and the *m-by-n* matrix $\mathbf{C}_d$ is computed from the finite element mass, damping, and stiffness matrices. An important restriction in the development which follows is that the dynamical system of Eqns (1) & (2) is completely state observable [10].

Deterministic Observer

The system is assumed to be completely deterministic and hence the measurement noise is taken as zero. Assume that an estimate of the state at any time i is available as $\hat{\mathbf{x}}(i)$, so that an estimate of the measurements is available from Eqn (2). From the actual measurements and the estimated measurements, a measurement error can be computed. The full-state observer is formed by multiplying the measurement error vector by a gain matrix and feeding it back into the state equation.

$$\hat{\mathbf{x}}(i+1) = \mathbf{A}_d\hat{\mathbf{x}}(i) + \mathbf{K}(\mathbf{y}(i) - \hat{\mathbf{y}}(i)) = \mathbf{A}_d\hat{\mathbf{x}}(i) + \mathbf{K}(\mathbf{y}(i) - \mathbf{C}_d\hat{\mathbf{x}}(i)) \qquad (3)$$

$$\hat{\mathbf{x}}(i+1) = (\mathbf{A}_d - \mathbf{KC}_d)\hat{\mathbf{x}}(i) + \mathbf{K}\mathbf{y}(i) \qquad (4)$$

Eqn (3) is the fundamental equation for both the deterministic observer and the Kalman filter and it is evident that the estimator is both recursive and linear in the measurement vector. With a little algebra it can be shown that the time behavior of the error vector (the true state minus the estimated state) is determined by the eigenvalues of the matrix $(\mathbf{A}_d - \mathbf{KC}_d)$. Therefore, one can choose the estimator performance by choosing the measurement error feedback matrix, $\mathbf{K}$. Furthermore, given a completely observable system, all eigenvalues of the system can be placed in arbitrary locations.

Design of the observer is carried out by specifying eigenvalue locations using engineering judgement, then the performance is checked through simulation. Eigenvalue locations can be adjusted until desired performance is achieved. Although it is true that under certain conditions the eigenvalues can be placed at arbitrary locations, it is usually left to engineering judgement to find the best locations. The gain matrix that achieves the desired eigenvalue locations can be calculated from the MATLAB function *place*. Finally, note from Eqn (4) that any noise in the measurements will be amplified by the gain matrix $\mathbf{K}$, so that the larger the gain matrix (the faster the eigenvalues), the larger the amplification of the noise.

Kalman Filter

The Kalman filter is an optimal estimator that seeks a minimum variance of the state error vector, given *a priori* knowledge of the measurement noise statistics. In addition to the measurement noise statistics, which are assumed to be white with covariance matrix, $\mathbf{R}$, we define the state error covariance matrix $\mathbf{P}$. The differences between the deterministic observer and the Kalman filter lie in how the gain matrix $\mathbf{K}$ is calculated, and that the state estimate at $i+1$ is *conditioned* on the measurement at $i+1$. The essential equations of the filter are:

$$\mathbf{x}(i+1|i+1) = \mathbf{A}_d x(i|i) + \mathbf{K}(i+1)\left[\mathbf{y}(i+1) - \mathbf{C}_d^T\mathbf{A}_d x(i|i)\right] \qquad (5)$$

$$\mathbf{K}(i+1) = \mathbf{P}(i+1|i)\mathbf{C}_d^T\left[\mathbf{C}_d\mathbf{P}(i+1|i)\mathbf{C}_d^T\mathbf{R}(i+1)\right]^{-1} \qquad (6)$$

$$\mathbf{P}(i+1|i) = \mathbf{A}_d^T\mathbf{P}(i|i)\mathbf{A}_d \qquad (7)$$

$$\mathbf{P}(i+1|i+1) = \left[\mathbf{I} - \mathbf{K}(i+1)\mathbf{C}_d^T\right]\mathbf{P}(i+1|i) \qquad (8)$$

Eqn (6) shows how the gain matrix is a function of both the

covariance of the error vector and the statistics of the measurement noise.

State estimation is a somewhat involved topic with an interesting and illustrious history and only the essential equations and ideas have been presented here. Additional information on both the Luenberger observer and the Kalman filter can be found in textbooks such as[10].

3. EXAMPLE

The second Interferometry Program Experiment (IPEX-II) is a space flight experiment investigating the microdynamic behavior of a representative deployed truss structure. This experiment serves as a technology demonstration for the planned space telescopes in NASA's Origins Program, including the Space Interferometry Mission (SIM). IPEX-II was flown on the STS-85 Shuttle Mission in August 1997, as a secondary payload mounted on the free-flying DARA/DASA satellite pallet, ASTRO-SPAS. One of the main objectives of this experiment is to demonstrate and characterize the occurrence of impulsive microdynamic-level disturbances, as a result of changes in the internal stress distribution of a structure with nonlinear frictional mechanisms.

The IPEX-II deployed truss is a nine-bay truss structure that was launched in the fully deployed state. Truss longerons and battens are constructed of graphite/epoxy composite rods connected at stainless steel nodes and the diagonal elements are prestressed stainless steel cables. Because the truss was launched in the deployed configuration, the pulley/latch mechanisms at the intersection of cable diagonals are locked. Total truss length is 2337 mm and total mass is 38.8 kg. Six interface support struts connect the truss to the ASTRO-SPAS satellite pallet. The truss is instrumented with 22 accelerometers (16 on the truss and six in the interface struts), six load cells (in the interface struts), thermistors, and two proof-mass actuators located at the truss free end for conducting on-orbit system identification (Figure 1). Additional information on the IPEX-II experiment can be found in [3].
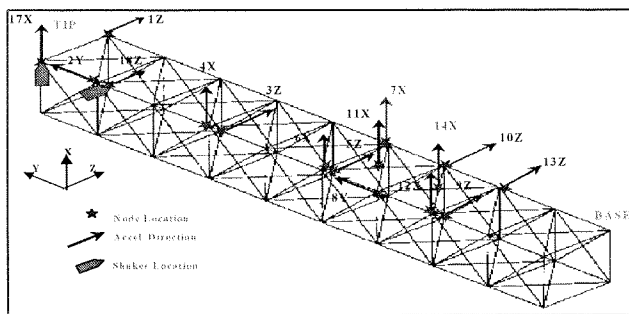

Figure 1 Instrumentation layout.

A coupled ASTRO-SPAS and truss structure finite element model was developed in UAI NASTRAN. The truss model is comprised of beam elements, plate elements, and lumped masses, and has 1289 elements and 5946 DOFs. The model is a linearization of the truss about its preloaded configuration, and standard Euler-Bernoulli beam elements are used to represent the prestressed diagonal cables. The truss model is coupled to a reduced-order

model of the ASTRO-SPAS pallet to bring the total DOF count to 6276. This is a preliminary model that has not yet been correlated with the on-orbit system identification experiments, but this is planned as a future activity.

A reduced-order model using Guyan reduction has been formed from the complete coupled model by retaining all the ASTRO-SPAS DOFs as well as translations at the corner nodes of the truss. The reduced model has 363 DOFs. A summary of the full-order finite element modes below 100 Hz is given in Table 1. Using the accelerometer locations shown in Figure 1, the system is completely observable. Note that because the associated nodes have been condensed out during Guyan reduction, the two accelerometers at diagonal pulley nodes are removed from the measurement set.

Table 1 FE Modes for Coupled IPEX/ASTRO-SPAS Model

Description B: boom bending T: boom torsion	Frequencies (Full-order FE model)
B1	12.53
B1	18.37
T1	28.21
SPAS-Dominated modes (coupled with boom bending and torsion)	34.81 39.81 41.18 48.47
Diagonal cable drum modes (coupled with B & T and SPAS deformation)	54.80 to 97.68

One possible source of microdynamic disturbances on-orbit is microslip at joints. The sudden appearance and free vibration decay characteristic of these events can be approximated in a simple way by the sudden release of the structure from a deformed shape. As an illustration of the state estimator approach, the initial condition for the following simulations is arbitrarily chosen as a linear combination of the mode shapes of the two modes at 39.81 and 41.18 Hz, modes which are ASTRO-SPAS dominated coupled with truss torsion and bending. The initial shape is then scaled so that the maximum displacement of any of the nodes on truss is 2.5E-6 meters, a value that is comparable with the actual measured on-orbit displacements. This initial deformed shape is shown in Figure 2. Although time histories are computed for all 363 DOFs in the model, only the responses at the measurement DOFs are used in the state estimators. The unmeasured DOFs are used to assess the accuracy of the state estimates.
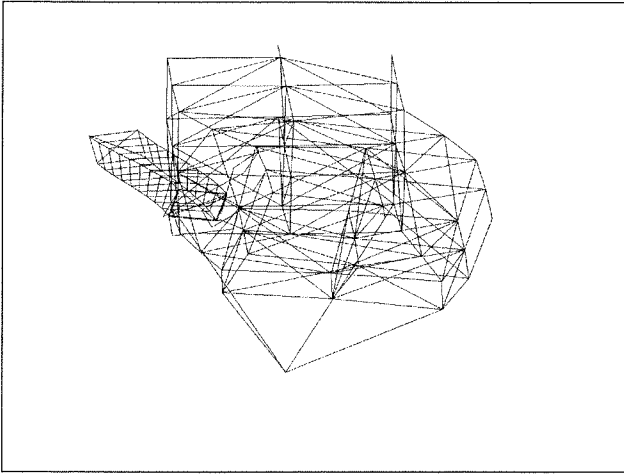
Figure 2 Initial deformed shape (amplified for emphasis).

Deterministic Observer

In the first set of simulations, we investigate the effect of measurement noise. In the second set of simulations, the measurements are noise-free, but systematic modeling errors in the finite element are assumed. Simulations were made with two different observer designs. In the *fast* observer, the observer eigenvalues were made faster than the finite element model eigenvalues by a factor of two, and observer damping was increased to 55% of critical. The *slow* observer used poles 1.5 times faster and 55% critical damping. Although these are not optimal eigenvalue locations in a rigorous sense, they were selected because they can be calculated accurately by MATLAB's place function (some pole locations lead to numerical ill-conditioning) and they result in adequate performance in the absence of noise.

Realistic noise statistics for these simulations were obtained from the actual IPEX flight data recordings. Root-mean-square noise levels of 24 µg to 41 µg were calculated, depending on the channel number, and were stationary throughout the time interval investigated. The noise is non-white, having distinct peaks in the PSD at 9, 18, 27, 75, 150, 190, and 360 Hz. The noise signals obtained from the flight data were simply scaled by a constant value (0.10 for 10% noise, for example), then time-domain added to the simulated signals at the measurement DOFs. No effort was made to adjust or align the phase of the noise with respect to the signal.

The quality of the estimated states from both observers is summarized in Table 2. In that table, the displacement error is defined as the true simulation displacements minus the displacements estimated from the observer at each node, squared, summed up along the simulation time, then summed across all nodes, to give a single mean-square number for the entire structure. The relative error is the mean-square displacement error divided by the total mean-square displacement, so relative errors greater than one indicate extremely poor estimates. Low relative errors confirm the accuracy of both observers for noise free measurements, with the fast observer performing marginally better. The high relative error as noise is added clearly show the sensitivity to measurement noise. Not shown in the tabulated results is the very large overshoot that occurs in the first few time points of the estimate – the magnitude of which increases with increasing speed of the observer poles. For this reason, the first thirty points of the estimated state vector have been ignored in computing the error levels shown in all tables.

Table 2 Deterministic observer performance with perfect models.

Fast Observer	added noise		
	0	10%	20%
total disp (m²)	2.06E-08	2.06E-08	2.06E-08
disp error (m²)	3.99E-13	8.44E-07	3.37E-06
relative error	1.94E-06	40.9	163.7
Slow Observer	added noise		
	0	10%	20%
total disp (m²)	2.06E-08	2.06E-08	2.06E-08
disp error (m²)	9.63E-13	4.41E-09	1.76E-08
relative error	4.67E-05	0.21	0.85

Table 3 Deterministic observer performance with imperfect model.

Slow Observer	1.1Kaa	1.9Kaa
total disp (m²)	1.91E-08	1.32E-08
disp error (m²)	2.87E-08	2.54E-06
relative error	1.5	192

For the second simulations, the slow observer is used but a systematic modeling error is introduced into the simulation finite element model. Specifically, the stiffness matrix Kaa is scaled by a constant value, either 1.1 or 1.9. This alters the frequencies but leaves the eigenvectors unchanged. Whereas the factor of 1.1 might represent a reasonable error in the model, the 1.9 scale factor is chosen to bring the first truss torsion mode at 28.2 Hz up to 41 Hz. In this case, the initial condition used in the simulation and presented to the observer is the truss torsion mode shape of the 41 Hz mode in the simulation model, which, at the measurement DOFs, has a very similar shape to the 38 and 41 Hz modes of the original model and the observer. Thus, this tests the ability of the observer to distinguish between modes of similar shapes at different frequencies. The results in Table 3 show the observer's lack of robustness with respect to modeling errors.

Kalman Filter

The same two sets of simulations were repeated with the Kalman filter and the results are reported in Tables 4 and 5. The very small errors in relative displacement indicate excellent filter performance, even in the presence of realistic noise that is non-white and correlated.

Figure 3 shows the spectrum of displacements at measurement channel 6, located at approximately the mid-point of the truss. The upper curve shows the frequency-domain double-integrated values of the simulated acceleration signal contaminated by 100% noise levels. Note the peaks in the spectrum at the noise frequencies of 9, 18, 27, and 75Hz, and especially how the low-frequency noise components are amplified by the integration

process until they dominate the signal amplitudes. Compare this to the estimated displacements from the Kalman filter, which shows a broad-band reduction in noise and does not suffer from this phenomenon.

A comparison of the estimated response and its associated error for an unmeasured DOF is shown in Figure 4 and Figure 5. This is a node located at the three-quarter point along the truss. The time behavior of the estimate shows the same smooth decay as the true state does, but the overshoot is clearly seen in the error signal (Figure 5). Estimated response of the same unmeasured DOF to the same excitation is shown in Figure 6 for the Kalman filter based on the imperfect model. The quality of the estimate varies among the DOFs, but what is shown is representative, with errors in amplitude and other mismatches in waveform.

Table 4 Performance of Kalman Filter with perfect model.

	added noise		
	10%	20%	100%
total disp (m^2)	1.73E-11	1.73E-11	1.73E-11
disp error (m^2)	1.12E-18	4.22E-18	1.07E-16
relative error	6.49E-08	2.45E-07	6.22E-06

Table 5 Kalman Filter with imperfect model.

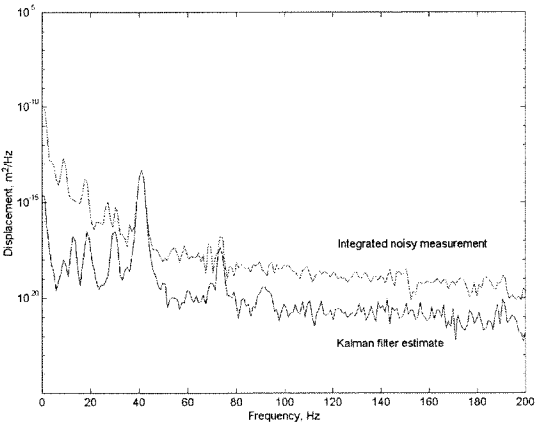|	1.1Kaa	1.9Kaa
total disp (m^2)	1.65E-11	1.27E-11
disp error (m^2)	1.54E-11	2.71E-11
relative error	0.937	2.13645

Figure 3 Power spectral density functions of measurement channel 6.
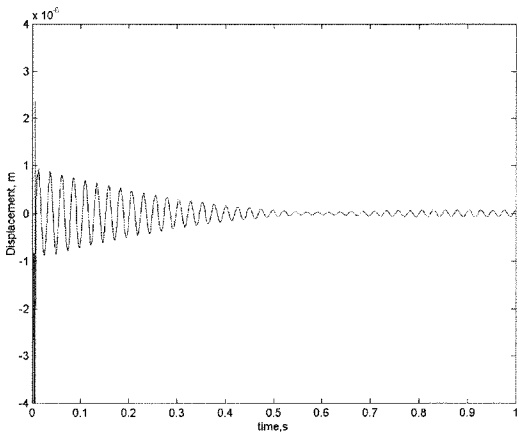

Figure 4 Estimated state predicted by the Kalman filter using a perfect model, at an *unmeasured* DOF.
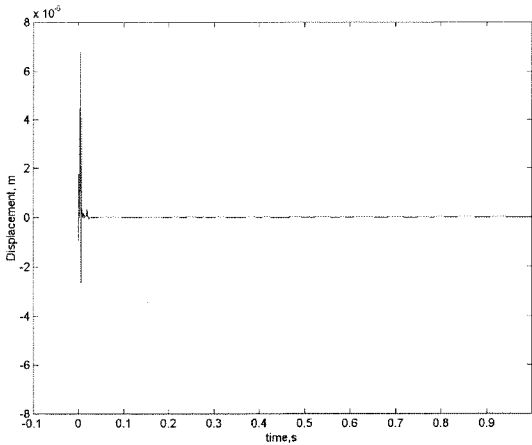

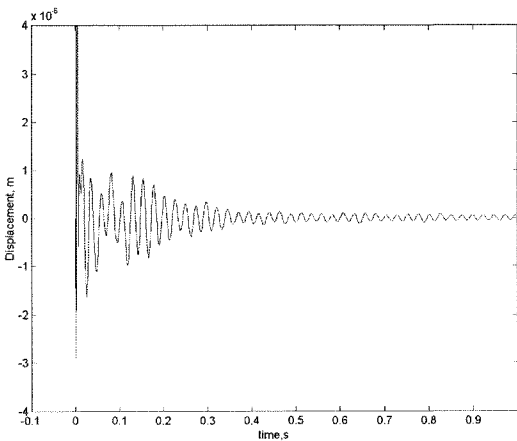Figure 5 Error in unmeasured estimated state of Figure 4.

Figure 6 Estimated state of Figure 4 using imperfect model (1.1Kaa).

4. CONCLUSION

Simulation results show that with the current pole location technique, the deterministic observer is too sensitive to noise and therefore must be considered unsuitable for reliably expanding measured time histories. The Kalman filter is much less sensitive to noise and was able to make essentially error-free state estimates if given a perfect model of the structure.

Although it could be argued that the modeling errors investigated here do not represent realistic finite element modeling errors, our results nevertheless show the desirablity, if not the need, for accurate finite element models.

The overshoot at the start of the estimated time histories obviously has negative implications for visualizing the deformed shape immediatley after a snap event, which was one of the goals of this study. Potential solutions currently under investigation include running the filter backwards in time, and implementing the filter as a smoother, whereby the current estimate of the state is conditioned not just on the current measurement, but all measurements, before and after the current instant.

The Kalman filter algorithm will next be applied to the IPEX experimental data to study transients that are associated with the tape recorder and occur at regular intervals. As confidence is increased and the approach is fine-tuned, additional events in the measured data will be studied in an attempt to relate measured responses with source locations.

5. ACKNOWLEDGEMENTS

6. REFERENCES

1. M. Levine, M. Milman, and A. Kissil, "*Mode Shape Expansion Techniques for Prediction: Experimental Evaluation*", AIAA Journal, Vol. 34, No. 4, April 1996.
2. Kalman, R., "*A New Approach to Linear Filtering and Prediction Problems*", Transactions of the ASME - Journal of Basic Engineering, March 1960, pp- 35-45.
3. M. Levine, "*On-Orbit Microdynamic Behavior of a Flexible Structure: IPEX II*", Proceedings of the International Modal Analysis Conference (IMAC) XVII, Kissimmee, FL, Feb 8-11, 1999.
4. Guyan, R.J., "*Reduction of Stiffness and Mass Matrices*", AIAA Journal, Vol. 3, No. 2, June 1965.
5. Irons, B.M. "*Structural Eigenvalue Problems: Elimination of Unwanted Variables*", AIAA Journal, Vol. 3, No. 2, May 1965.
6. O'Callahan, J. "*A procedure for an improved reduced system (IRS)*", Proceedings of the 7th International Modal Analysis Conference (IMAC), 1989.
7. Wilson, E.L., M-W. Yuan, and J.M. Dickens. "*Dynamic analysis by direct superposition of Ritz vectors*", Earthquake Engineering and Structural Dynamics, Vol. 10, 1982.
8. Craig, R.R. and T-J. Shu. "*A Review of model reduction techniques for structural control design*", In C.L. Kirk and J.L. Junkins, eds. Dynamics of Flexible Structures in Space, Springer-Verlag, 1990.
9. Luenberger, D.G. "*Observing the State of a Linear System*", IEEE Transactions on Military Electronics, Vol. MIL 8, April 1964.
10. Brammer, K. and G. Siffling, "*Kalman-Bucy Filters*", Artech House, 1989.